Journal of Alloys and Compounds 511 (2012) 129–132

Contents lists available at SciVerse ScienceDirect

Journal of Alloys and Compounds

journal homepage: www.elsevier.com/locate/jallcom

Composition dependence of structure and optical properties of $Cu_2ZnSn(S,Se)_4$ solid solutions: An experimental study

Jun He, Lin Sun*, Shiyou Chen, Ye Chen, Pingxiong Yang, Junhao Chu

Key Laboratory of Polar Materials and Devices, Ministry of Education, East China Normal University, Shanghai 200241, China

ARTICLE INFO

Article history:
Received 8 July 2011
Received in revised form 29 August 2011
Accepted 31 August 2011
Available online 10 September 2011

Keywords:
$Cu_2ZnSn(S,Se)_4$
X-ray diffraction (XRD)
Raman spectroscopy
Optical absorption
Solid solutions

ABSTRACT

The evolution of structure and optical properties of Cu_2ZnSn $(S_xSe_{1-x})_4$ (CZTSSe) solid solutions in a wide composition range ($0 \le x \le 1$) has not been fully elucidated. We have performed comprehensive characterization on the CZTSSe powders with different S/Se ratios, which were synthesized by the solid state reaction method. X-ray diffraction patterns demonstrate that the lattice parameters a and c of CZTSSe decrease lineally when S replace Se gradually, which obeys the Vegard's rule. The A_1 Raman modes of CZTSSe show a typical two-mode behavior. The absorption spectra reveal that the band gap of CZTSSe can be tuned monotonously between 0.96 and 1.5 eV with almost linearity, and a small band gap bowing constant ($b \approx 0.08$ eV) is deduced.

1. Introduction

In recent years, quaternary semiconductor Cu_2ZnSnS_4 (CZTS), $Cu_2ZnSnSe_4$ (CZTSe) and their CZTSSe solid solutions for a novel absorber layer of thin film solar cells have attracted great interest due to their high absorption coefficients (>10^4 cm^{-1}), an optimal direct band gap and the abundance of elements in the earth's crust [1,2]. For example, the record power conversion efficiencies (PCE) for CZTS and CZTSe solar cells have improved to 6.8% and 3.2% [3,4], respectively. More importantly, CZTSSe thin film solar cell fabricated by using a hydrazine-based solution process has attained the record PCE as high as up to 9.6% [5]. These research results demonstrate CZTSSe solid solutions have the great potential as an alternative absorber for CdTe or $Cu(In,Ga)Se_2$ thin film solar cells.

For high efficient thin film solar cells, the band gap (E_g) of the absorber layer is one of the important parameters. Several groups have reported that E_g can be tuned by changing the ratio of sulfur and selenium in CZTSSe solid solutions [6–8]. However, there still exists a discrepancy about the composition dependence of E_g. Wei et al. [6] have observed a parabolic relation of tunable band gaps from 1.28 to 1.5 eV, while Grossberg et al. [7] have obtained a linear dependence of band gap E_g by PL spectrum measurements. Chen et al. predict a near linear dependence of band gap on the S/Se ratio with a small bowing parameter by using first-principles calculations [8]. Thus, further experimental evidences are needed to clarify these debates. On the other hand, the miscibility mechanism of CZTSSe as the complicated multinary alloys is unclear. Chen et al. have also studied the structure of CZTSSe alloys through first-principles calculations [8]. Their calculations reveal the mixed-anion alloys are highly miscible. Unfortunately, up to date there is no systematical experiment report on the structure of CZTSSe alloys. Therefore, an experimental research on the structure and optical properties of CZTSSe solid solutions is essential to develop further the CZTSSe thin film solar cells. In this paper, CZTSSe solid solutions (i.e. alloys) were synthesized by the solid state reaction method. The composition dependence of structure and optical properties of CZTSSe solid solutions has been systematically investigated and our research results give the direct experimental evidence to the related theoretical calculations.

2. Experimental

CZTSSe powders with different S/Se ratios were synthesized with high pure $Cu_2S(Se)$, $ZnS(Se)$, SnS_2, Sn, S, and Se powders by the solid state sintering method. Ratios of these initial powders are shown in Table 1. Considering that sulfur and selenium are volatile elements, all the starting powders were 5% sulfur and selenium in excess. The powders were ball-milled in ethanol for 8 h with the speed of 350 r/min, and these mixed powders were dried in a non-vacuum evaporator at 50 °C. The dried powders were pressed into pellets by a mold and then pre-sintered at 500 °C for 2 h using tubular furnace under Ar gas flow. The heating and cooling rates were 5 °C/min. After the pre-sintered process was finished, the furnace was allowed to cool to room temperature. The sintered pellets were ground into powders in mortar and finally sintered at 700 °C to obtain CZTSSe polycrystalline powders. The crystalline structures of the CZTSSe powders were analyzed by X-ray diffraction (XRD) using Cu Kα radiation (Rigaku DMAX2500, Japan) from 10° to 70°. Raman scattering experiments were performed with a micro-Raman spectrometer (Jobin-Yvon LabRAM HR 800UV). The compositions of these powders

* Corresponding author. Tel.: +86 21 54345123; fax: +86 21 54345119.
E-mail addresses: lsun@ee.ecnu.edu.cn, bolissun@hotmail.com (L. Sun).

0925-8388/$ – see front matter © 2011 Elsevier B.V. All rights reserved.
doi:10.1016/j.jallcom.2011.08.099

Table 1
Composition of initial powders and atomic ratios of Cu/(Zn + Sn), Zn/Sn, metals/(S + Se), S/(S + Se) of the $Cu_2ZnSn(S_xSe_{1-x})_4$ powders. *x* symbolizes the S/(S + Se) ratios.

Initial powders	Sample	Cu/(Zn + Sn)	Zn/Sn	Metals/(S + Se)	S/(S + Se)
$Cu_2Se + ZnSe + Sn + 2Se$	I	0.81	1.70	1.31	0
$Cu_2S + ZnSe + Sn + 2Se$	II	1.18	1.52	1.54	0.23
$Cu_2Se + ZnSe + Sn + 2S$	III	1.09	1.42	1.19	0.49
$Cu_2S + ZnSe + SnS_2$	IV	1.05	1.12	1.55	0.69
$Cu_2S + ZnS + SnS_2$	V	0.94	1.03	1.20	1

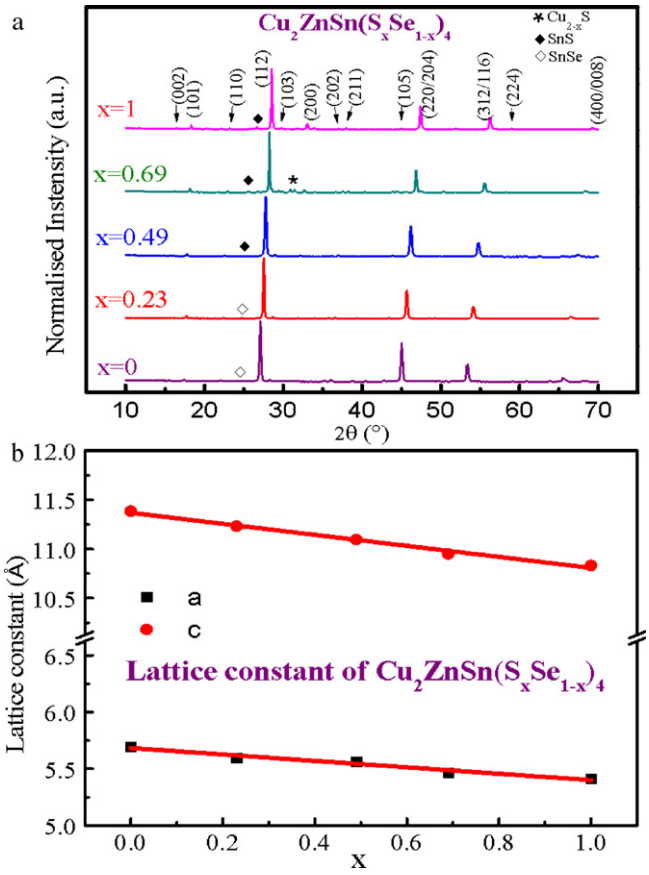

Fig. 1. (a) XRD patterns of $Cu_2ZnSn(S_xSe_{1-x})_4$ powders with different *x* values; (b) lattice constant of $Cu_2ZnSn(S_xSe_{1-x})_4$ with varying *x* values and the solid lines represent linear fits.

were determined by Energy dispersive X-ray spectroscopy (EDX) (HITACHI s-4700). The optical absorption experiments were carried out by ultraviolet–visible–near-infrared (UV–vis–NIR) spectrophotometer (cary500, USA Varian) equipped with integrating sphere.

3. Results and discussion

The elemental compositions deduced from EDX measurements are shown in Table 1 in terms of Cu/(Zn + Sn), Zn/Sn, metals/(S + Se), and S/(S + Se) ratios. From composition analysis, it is found that there are more losses of Sn than Zn with increasing the Se content in CZTSSe samples. It is probably due to the fact that Sn is easily lost by evaporation of SnSe phases at temperatures higher than 400 °C [9,10]. By means of EDX measurements, S/(S + Se) ratios (i.e. *x*) for Samples I, II, III, IV and V are determined to be 0, 0.23, 0.49, 0.69 and 1.0, respectively.

Fig. 1 presents the XRD patterns of CZTSSe powders. For all samples three dominant peaks (1 1 2), (2 0 4) and (3 1 2) are attributed to the CZTS compound, in terms of the standard XRD patterns (JCPDS 26-0575 for CZTS). Furthermore, it can be obviously observed that these diffraction peaks move to higher angles regularly when the S content increases, since the replacement of small S for large Se

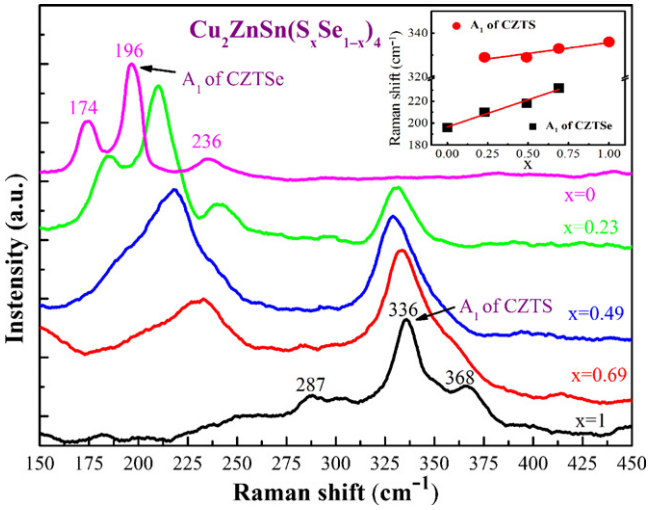

Fig. 2. Raman spectra for $Cu_2ZnSn(S_xSe_{1-x})_4$ samples. The inset is A_1 Raman mode frequency dependence on *x* values and the solid lines represent linear fits.

atoms makes the lattice shrink. This XRD analysis indicates that the S element can easily replace the Se element with the arbitrary S/Se ratio and form the CZTSSe solid solutions.

CZTSSe alloys have tetragonal crystal structure, and thus their lattice parameters (*a* and *c*) can be easily calculated from XRD patterns shown in Fig. 1(a). Fig. 1(b) shows the calculated a and c of CZTSSe samples (i.e. *x* = 0, 0.23, 0.49, 0.69, and 1), which are derived from their XRD patterns. For instance, *a* and *c* of CZTSe are 5.6955 and 11.3847 Å, while those of CZTS are 5.4111, 10.8313 Å, respectively. These values are very close to the reported lattice parameters of CZTS and CZTSe [11,12]. Moreover, as shown in Fig. 1(b), the variational trend of lattice parameters for CZTSSe alloys obeys Vegard's rule [13]:

$$a(x) = xa(A) + (1 + x)a(B), \quad (1)$$

where *a* is the lattice parameters (including *a* and *c* of CZTSSe), *A* is CZTS (i.e. *x* = 1) and *B* is CZTSe (i.e. *x* = 0). The lattice constants (i.e. *a*, *c* of CZTSSe) decrease linearly with increasing the S content in CZTSSe solid solutions.

Raman spectroscopy is also useful to analyze the structure and the phase purity of CZTSSe samples besides XRD analysis. Fig. 2 shows the Raman spectra of CZTSSe samples measured at room temperature. It can be clearly seen that the main Raman peaks of CZTS (i.e. *x* = 1) are detected at 287, 336 and 368 cm^{-1}, while those of CZTSe (i.e. *x* = 0) appear at 174, 196 and 236 cm^{-1}. This observation is consistent with the published data in the literature [14,15]. In addition, no Raman peaks of the secondary phase are obviously observed in the Raman spectra, implying the absence of obvious impurity phases in CZTSSe solid solutions. From the vibration viewpoint, the zone center phonon representation of CZTSe or CZTS structure is composed of 24 vibration modes [16,17], including 3 acoustic modes and 21 optical modes. Since some vibration modes among 21 optical modes are Raman active, only Raman peaks corresponding to these modes are possibly detected in Raman scattering measurement. Among these Raman active modes, the A_1 vibration

mode originates from the vibrations of S or Se atom surrounded by the other atoms at rest in the lattice and this mode is generally expected to correspond to the dominant peak in the Raman spectra [14]. Thus the Raman peaks at 196 cm^{-1} for CZTSe sample and 336 cm^{-1} for CZTS sample are ascribed to the A_1 mode. Fig. 2 also shows that the Raman spectra of CZTSSe with intermediate values (i.e. $x = 0.23$, 0.49, and 0.69) exhibit a two-mode behavior due to the coexistence of S and Se atoms in CZTSSe samples. It is apparent that these two modes, A_1 modes of CZTS and CZTSe, shift continuously toward the high frequency direction with increasing the sulfur content for CZTSSe samples.

A_1-mode frequency dependences on the sulfur content in CZTSSe solid systems are presented in Fig. 2 (inset). As shown in the inset of Fig. 2, with increasing the sulfur content in CZTSSe samples, the A_1 modes of CZTSe and CZTS shift approximately linearly toward the high frequency direction. This interesting observation can be illustrated by the mass effect and the change of the bond strength. According to the extended Keating's model, the frequency of the A_1 mode is given by [18,19]:

$$\nu = \sqrt{\frac{2\alpha_{Cu-VI} + \alpha_{Zn-VI} + \alpha_{Sn-VI}}{M_{VI}}}, \quad (2)$$

where α_{X-VI} (i.e. X = Cu, Zn, Sn and VI = S, Se) are the bond-stretching force constants related to the interaction between the nearest neighbors, and M_{VI} is the mass of S or Se. On the one hand, the atomic mass of S is lighter than that of Se ($M_{Se} = 78.96$, $M_S = 32.066$). Hence, the frequency of A_1 mode should move gradually to higher frequencies when S replaces partially Se atoms in CZTSSe solid solutions [20]. On the other hand, these bond-stretching force constants α_{X-VI} depend on the nearest-neighbor cation–anion bond length, and the relationship can be expressed by the following equation [21]:

$$\alpha_{X-VI} = a_1 d^{-x}, \quad (3)$$

where a_1 and x are constants, d is the bond length, which represents the nearest-neighbor cation–anion distance. Within the family of tetrahedral compounds the x values varying in the range from 2.3 to 3.0 [22]. XRD analysis above has demonstrated that the lattice constants of CZTSSe samples shrink gradually with the increase in the sulfur content, indicating that the bond lengths shorten when S substitutes partially for Se atoms. In terms of Eq. (3), the bond-stretching force constants of CZTSSe will become stronger when S substitutes gradually for Se. Thus the A_1 modes of CZTSe and CZTS will shift toward the higher frequency direction with increasing the S content, due to the increase in the bond-stretching force constants for CZTSSe solid solutions. Therefore, the combination of lower mass and stronger bond strength makes A_1 modes of CZTS and CZTSe frequency move toward the higher frequency direction with increasing the S content in CZTSSe solid solutions.

For CZTSSe powders, their absorption coefficients cannot be measured directly but the "absorbance" can be measured by diffuse reflection spectroscopy. It should be emphasized that the "absorbance" is equivalent to the absorption coefficient for powder samples. If A, α, c and l symbolize the absorbance, absorption coefficient, concentration and thickness for sample, respectively, there is a following equation: $A = \alpha \times c \times l$. For CZTSSe powder samples, $c = 1$, and l is the same values for all measured samples. So the measured value "absorbance" just represents the absorption coefficient. Fig. 3 shows the optical absorption spectra of the CZTSSe powders using UV–vis–NIR spectrophotometer. It is apparent that the band-edge absorptions of the CZTSSe powders exhibit gradually a blue shift (i.e. move toward shorter wavelength) with increasing the S content. This is due to the fact that the E_g of CZTSe is smaller than that of CZTS. It is interesting to note that the infrared absorption below band-edge increases gradually while the ultraviolet–visible

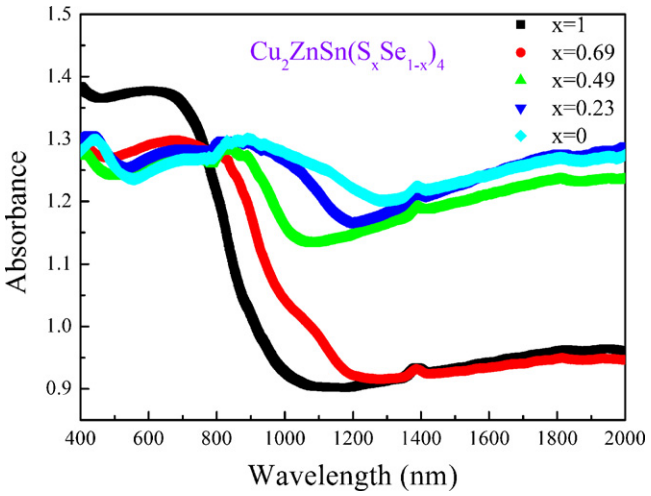

Fig. 3. Absorption spectra of $Cu_2ZnSn(S_xSe_{1-x})_4$ powders.

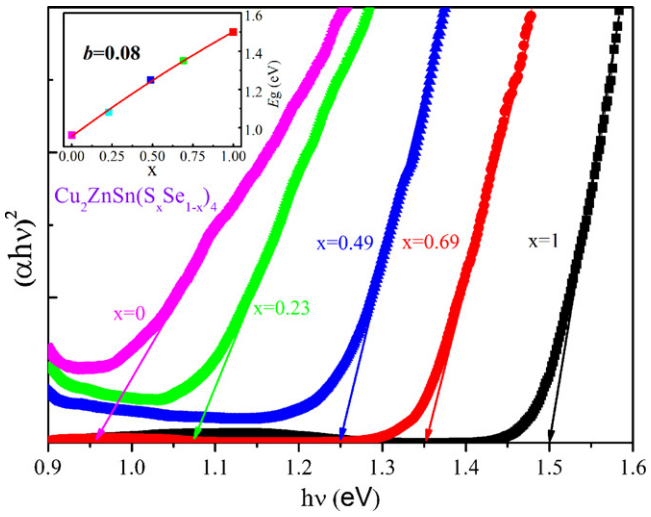

Fig. 4. Band gap determination plot of $Cu_2ZnSn(S_xSe_{1-x})_4$ powders. The inset gives the optical bowing constant b obtained by the fitting method.

absorption above band-edge decreases gradually with increasing the Se content for CZTSSe samples. The increase in the absorption below band-edge is probably related to the more impurity defects (i.e. the vacancies of Sn) in CZTSSe samples with higher Se content, because EDX results shown in Table 1 have demonstrated that the content of Sn decreases gradually with increasing the Se content. The decrease in the absorption above band-edge may be due to the difference on the absorption coefficients between CZTS and CZTSe. To our knowledge, there is no definite comparison of absorption coefficients between them up to now. Our experimental results may imply that the absorption coefficient of CZTS is higher than that of CZTSe.

CZTS and CZTSe are direct band gap materials and these E_g values of CZTSSe powers are obtained by extrapolating the linear $(\alpha h\nu)^2$ versus $h\nu$ plots to the horizontal axis, where α is the absorption coefficient and $h\nu$ is the photon energy. The value of vertical axis in Fig. 4 begins from zero in order to determine the E_g values accurately. These E_g values of the CZTSSe powders with different S/Se ratios are shown in Fig. 4. As shown in Fig. 4, these determined E_g values of five CZTSSe samples ($x = 0$, 0.23, 0.49, 0.69, and 1) are 0.96, 1.08, 1.25, 1.35, and 1.5 eV, respectively. The detailed method to obtain the E_g can be available in the supplementary material of Ref. [23]. These E_g values of CZTS (i.e. $x = 1$) and CZTSe (i.e. $x = 0$)

agree well with the reported values [24–27]. Furthermore, the E_g of CZTSSe increases monotonically with the increase in the sulfur content. As we mentioned above, the composition dependence on the band gap of CZTSSe is in dispute. Our experimental results show that the evolution of the E_g of CZTSSe solid solutions can be described by the following equation:

$$E_g^{CZTSSe} = xE_g^{CZTS} + (1-x)E_g^{CZTSe} - bx(1-x), \quad (4)$$

where b is the specific optical bowing constant which describes the degree of nonlinearity. The bowing constant b can be obtained by the parabola fitting method. As shown in the inset of Fig. 4, the best fitting value is about 0.08 eV, which is consistent with the value of theoretical calculations (~0.1 eV) [8]. Small size and chemical difference between S and Se are responsible for the small bowing parameter [28]. Consequently, the investigation of the evolution of E_g of CZTSSe samples indicates that the E_g of CZTSSe can be controlled almost linearly by varying the ratio of S/Se because of the small bowing constant.

4. Conclusion

The CZTSSe solid solutions were synthesized by solid state reaction method. EDX, XRD and Raman spectra reveal that the atomic Se and S are highly miscible in CZTSSe solid solutions. With the increase in the sulfur content, the lattice parameters a and c of CZTSSe shrink lineally and obeys the Vegard's rule. The A_1-mode Raman peaks of CZTSe and CZTS move to the higher frequency with increasing the S content, which is caused by the mass effect and the different bond-stretching force constant. The absorption spectra show that the band gaps of CZTSSe solid solutions increase almost linearly with the increase in the S content. A small band gap bowing constant ($b \approx 0.08$ eV) is obtained. These experimental results agree well with the theoretical prediction by the first-principles calculation. We expect that our research can be helpful to elucidate the evolution of structure and band gaps of CZTSSe with the change of S content.

Acknowledgments

The authors are grateful to the measurement of Professor Zhigao Hu group in Raman scattering spectra. This project was financed by specialized Research Fund for the Doctoral Program of Higher Education of China (Grant No. 20100076120009), the Science and Technology Commission of Shanghai Municipality Project (Grant Nos. 11ZR1411400, 10DJ1400200 and 10JC1404600), the National Natural Science Foundation of China (10874127, 60990312 and 61076060) and PCSIRT in University.

References

[1] K. Ito, T. Nakazawa, Jpn. J. Appl. Phys. 27 (1988) 2094.
[2] H. Katagiri, K. Saitoh, T. Washio, H. Shinohara, T. Kurumadani, S. Miyajima, Sol. Energy Mater. Sol. Cells 65 (2001) 141.
[3] H. Katagiri, K. Jimbo, W.S. Maw, K. Oishi, M. Yamazaki, H. Araki, A. Takeuchi, Thin Solid Films 517 (2009) 2455.
[4] G. Zoppi, I. Forbes, R.W. Miles, P.J. Dale, J.J. Scragg, L.M. Peter, Prog. Photovolt.: Res. Appl. 17 (2009) 315.
[5] T.K. Todorov, K.B. Reuter, D.B. Mitzi, Adv. Mater. 22 (2010) 1.
[6] H. Wei, Z. Ye, M. Li, Y. Su, Z. Yang, Y. Zhang, Cryst. Eng. Commun. 13 (2011) 2222.
[7] M. Grossberg, J. Krustok, J. Raudoja, K. Timmo, M. Altosaar, T. Raadik, Thin Solid Films 519 (2011) 7403.
[8] S. Chen, A. Walsh, J. Yang, X.G. Gong, L. Sun, P.X. Yang, J.H. Chu, S.H. Wei, Phys. Rev. B 83 (2011) 125201.
[9] P.M.P. Salomé, P.A. Fernandes, A.F. da Cunha, Phys. Stat. Sol. C 7 (2010) 913.
[10] A. Redinger, S. Siebentritt, Appl. Phys. Lett. 97 (2010) 092111.
[11] H. Katagiri, N. Sasaguchi, S. Hando, S. Hoshino, J. Ohashi, T. Yokota, Sol. Energy Mater. Sol. Cells 49 (1997) 407.
[12] H. Matsushita, T. Maeda, A. Katsui, T. Takizawa, J. Cryst. Growth 208 (2000) 416.
[13] L. Vegard, Z. Phys. 5 (1921) 17.
[14] A. Redinger, K. Hönes, X. Fontané, V. Izquierdo-Roca, E. Saucedo, N. Valle, A. Pérez-Rodríguez, S. Siebentritt, Appl. Phys. Lett. 98 (2011) 101907.
[15] K. Wang, O. Gunawan, T. Todorov, B. Shin, S.J. Chey, N.A. Bojarczuk, D. Mitzi, S. Guha, Appl. Phys. Lett. 97 (2010) 143508.
[16] M. Himmrich, A. Haeuseler, Spectrochim. Acta Part A 47 (1991) 933.
[17] N.B.M. Amiri, A. Postnikov, Phys. Rev. B 82 (2010) 205204.
[18] D. Papadimitriou, N. Esser, C. Xue, Phys. Stat. Sol. (b) 242 (2005) 2633.
[19] H. Neumann, Helv. Phys. Acta 58 (1985) 337.
[20] D.B. Mitzi, O. Gunawan, T.K. Todorov, K. Wang, S. Guha, Sol. Energy Mater. Sol. Cells 95 (2011) 1421.
[21] V. Kumar, D. Chandar, Phys. Stat. Sol. (b) 212 (1999) 37.
[22] H. Neumann, Cryst. Res. Technol. 24 (1989) 325.
[23] X. Lu, Z. Zhuang, Q. Peng, Y. Li, Chem. Commun. 47 (2011) 3141–3143.
[24] J.S. Seol, S.Y. Lee, J.C. Lee, H.D. Nam, K.H. Kim, Sol. Energy Mater. Sol. Cells 75 (2003) 155.
[25] F. Liu, Y. Li, K. Zhang, B. Wang, C. Yan, Y. Lai, Z. Zhang, J. Li, Y. Liu, Sol. Energy Mater. Sol. Cells 94 (2010) 2431.
[26] S. Ahn, S. Jung, J. Gwak, A. Cho, K. Shin, K. Yoon, D. Park, H. Cheong, J.H. Yun, Appl. Phys. Lett. 97 (2010) 021905.
[27] P.M.P. Salome, P.A. Fernandes, A.F. da Cunha, J.P. Leitao, J. Malaquias, A. Weber, J.C. Gonzalez, M.I.N. da Silva, Sol. Energy Mater. Sol. Cells 94 (2010) 2176.
[28] S.H. Wei, A. Zunger, J. Appl. Phys. 78 (1995) 3846.